The Cryosphere Discuss., 9, 6025–6060, 2015
www.the-cryosphere-discuss.net/9/6025/2015/
doi:10.5194/tcd-9-6025-2015

The Cryosphere Discussions
Open Access
EGU

A Retrospective, Iterative, Geometry-Based (RIGB) tilt correction method for radiation observed by Automatic Weather Stations on snow-covered surfaces: application to Greenland

W. Wang[1], C. S. Zender[1], D. van As[2], P. C. J. P. Smeets[3], and M. R. van den Broeke[3]

[1]Department of Earth System Science, University of California, Irvine, California, USA
[2]Geological Survey of Denmark and Greenland (GEUS), Copenhagen, Denmark
[3]Institute for Marine and Atmospheric Research, Utrecht University (UU/IMAU), Utrecht, the Netherlands

Received: 28 September 2015 – Accepted: 9 October 2015 – Published: 3 November 2015

Correspondence to: W. Wang (wenshanw@uci.edu)

Published by Copernicus Publications on behalf of the European Geosciences Union.

Abstract

Surface melt and mass loss of the Greenland Ice Sheet may play crucial roles in global climate change due to their positive feedbacks and large fresh water storage. With few other regular meteorological observations available in this extreme environment, measurements from Automatic Weather Stations (AWS) are the primary data source for studying surface energy budgets, and for validating satellite observations and model simulations. Station tilt, due to irregular surface melt and/or compaction, causes considerable biases in the AWS shortwave radiation measurements. In this study, we identify tilt-induced biases in the climatology of surface shortwave radiative flux and albedo, and retrospectively correct these by iterative application of solar geometric principles. We found, over all the AWS from the Greenland Climate Network (GC-Net), the Kangerlussuaq transect (K-transect) and the Programme for Monitoring of the Greenland Ice Sheet (PROMICE) networks, insolation on fewer than 40 % of clear days peaks within ±0.5 h of solar noon time, with the largest shift exceeding 3 h due to tilt. Hourly absolute biases in the magnitude of surface insolation can reach up to 200 $W m^{-2}$. We estimate the tilt angles and their directions based on the solar geometric relationship between the simulated insolation at a horizontal surface and the observed insolation by these tilted AWS under clear-sky conditions. Our adjustment reduces the Root Mean Square Error (RMSE) against references from both satellite observation and reanalysis by ~ 20 $W m^{-2}$, and raises the correlation coefficients with them to above 0.95. Averaged over the whole Greenland Ice Sheet in the melt season, the adjustment in insolation to compensate station tilt is 18 ± 13 $W m^{-2}$, enough to melt 0.40 ± 0.29 m of snow water equivalent. The adjusted diurnal cycles of albedo are smoother, with consistent semi-smiling patterns. The seasonal cycles and inter-annual variabilities of albedo agree better with previous studies. This tilt-corrected shortwave radiation dataset derived using the Retrospective, Iterative, Geometry-Based (RIGB) method provide more accurate observations and validations for surface

TCD
9, 6025–6060, 2015

energy budgets studies on the Greenland Ice Sheet, including albedo variations, surface melt simulations and cloud radiative forcing estimates.

1 Introduction

The Greenland Ice Sheet has experienced dramatic mass loss and frequent massive melt events in the past 30 years (Nghiem et al., 2012; Tedesco et al., 2013; Velicogna and Wahr, 2013). At least half of the mass loss can be attributed to surface mass balance (van den Broeke et al., 2009; Enderlin et al., 2014; Andersen et al., 2015), which is in turn controlled by solar radiation (van den Broeke et al., 2011). Therefore, reliable measurements of surface radiative flux are essential for climate change studies in this sensitive area (Pithan and Mauritsen, 2014). In this study, we correct the station tilt problem to produce more consistent shortwave radiation (thereafter, SW) measured by the Automatic Weather Stations (AWS).

In the highly cloudy arctic area (Vavrus et al., 2008), studies of surface energy budgets and mass loss rely on the in situ AWS measurements of surface radiative flux, since satellites cannot see through thick clouds, and have a large uncertainty at high solar zenith angles (Wang and Zender, 2010b; Schaaf et al., 2011). Stroeve et al. (2013) evaluated cloud-free albedo retrievals from the MODerate resolution Imaging Spectroradiometer (MODIS) Terra and Aqua combined 16-day albedo product (MCD43) against in situ measurements by AWS in Greenland. They found a negative trend in albedo during summer from 2000 to 2012, with a large negative anomaly in July 2012 (0.060 lower than the average of July 2000–2009: 0.627). Wang and Zender (2010a) adjusted MODIS MCD43 albedo retrievals over snow-covered regions in Greenland to remove the low bias at large solar zenith angles, based on snow optical properties and AWS radiation measurements. The resulting adjustments in absorbed solar radiation are as large as 8.0 and 10.8 % for the black-sky and white-sky albedo, respectively. Nevertheless, only AWS observe the all-sky albedo. van den Broeke et al. (2011) calculated the surface energy balance (SEB) and melt rate in the ablation

TCD
9, 6025–6060, 2015

zone of west Greenland using a SEB model driven by hourly AWS measurements. They found that the seasonal cycle and inter-annual variability of melt are mainly controlled by absorption of SW, except in the lower ablation zone where the turbulent fluxes of sensible and latent heat dominate. The AWS measurements are also used in various other applications, such as to estimate cloud radiative effects on surface albedo (Kuipers Munneke et al., 2011), and to validate regional climate model simulations (Fettweis, 2007; Box et al., 2012; van As et al., 2014).

These radiative fluxes measured by unattended stations may contain considerable biases (Stroeve et al., 2001; van den Broeke et al., 2004). In the assessment of AWS in Antarctica, van den Broeke et al. (2004) summarized the typical problems of SW measurements, including icing and riming of the sensor dome, cosine response error at large solar zenith angles, and sensor tilt. Other possible problems include the shadowing of the station tower or nearby high structures, and random micro-scale environmental noise (Stroeve et al., 2005). An ice coating over the sensor dome can shield part of the incoming solar radiation, causing an underestimate of net SW. Shadows on the sensor can also lead to an underestimate. On the other hand, riming on the sensor dome can increase the incoming solar radiation, especially at large solar zenith angles, due to the enhanced multi-scattering of the solar radiation, causing an overestimate of net SW. However, in the high and dry interior of ice sheets, icing and riming are not major problems due to the small thermal mass of the pyranometers (Stroeve et al., 2001). Moreover, the unlikely high/low values induced by the icing, riming and shadowing can be removed by detecting the sudden change of albedo since the down-looking sensors are generally less sensitive to these problems. The cosine response error at large solar zenith angles is intrinsic and can cause an underestimate in net SW in excess of 5 % for solar zenith angles larger than 75° (Stroeve et al., 2001).

The primary source of the bias in the SW is the instrument leveling (i.e., sensor tilt) (van den Broeke et al., 2004; van As, 2011; Stroeve et al., 2013). Different snow melt and compaction around the station towers and/or cable anchors can cause the station to drift over time. The tilted sensors will result in either underestimates or overestimates

TCD
9, 6025–6060, 2015

of radiation measurements, depending on the combination of the tilt angle and tilt direction. SW is quite sensitive to sensor tilt. Theoretically, a tilt angle of 1° towards 40° N will induce a $\sim 20\,W\,m^{-2}$ bias in net SW (van den Broeke et al., 2004). Using a radiative transfer model, Bogren et al. (2015) estimated the albedo error introduced by a station tilt of 5° to be ~ 13 %. Moreover, the diurnal phase of radiation will be shifted, suggesting that sub-daily variabilities will be inaccurate without correcting the tilt problem. Both van den Broeke et al. (2004) and Stroeve et al. (2013) used a 24 h running average as a workaround. van den Broeke et al. (2004) further calculated net SW by multiplying the 24 h running average albedo with the upwelling radiation, which is less susceptible to station tilt. These workarounds provide more stable estimates of radiation and albedo. However, the only way to obtain the accurate radiation and albedo at any time scales is to correct the tilt problem. The PROMICE AWS are equipped with inclinometers, measuring the north-south and east-west tilt angles. The station rotation is obtained every 1–2 years by re-visiting the station. Insolation observed by tilted AWS can then be adjusted using this information (van As, 2011). However, in spite of the effort to re-position the stations during each visit, the frequent station rotation, occurring together with station tilt, changes the orientation of these inclinometers, making the measured tilt angles questionable. Moreover, the tilt problem remains at half of the AWS in Greenland with no inclinometers at all.

For longwave radiation, the most important bias source is the window heating offset (van den Broeke et al., 2004), which occurs when the silicon window is warmer than the sensor housing, caused by an excess of solar radiation absorption. Although this problem cannot be removed without knowing the window temperature, the overall effect on net longwave radiation is less than $5\,W\,m^{-2}$ (van den Broeke et al., 2004), which is quite small relative to the shortwave bias caused by tilt discussed here.

To ameliorate tilt biases in SW measured by AWS, we introduce a new method – the Retrospective, Iterative, Geometry-Based (RIGB) tilt correction method – that depends only on solar geometry, and no additional instrumentation. Sections 2 and 3 describe the datasets we use, and RIGB method to estimate tilt angle-direction and to

TCD
9, 6025–6060, 2015

adjust SW. In Sect. 4, we evaluate our adjusted insolation against satellite observations and reanalysis at all stations, and against data from PROMICE stations, which were adjusted by the inclinometer-measured tilt angles. To what degree station tilt affects the diurnal phase and magnitude of insolation are also revealed in this section. In Sect. 5, we present the observed diurnal variability of albedo over Greenland for the first time, and show the improvement of the monthly and annual climatology using the adjusted SW. In Sect. 6, we explore the dominant factors for station tilt, and discuss the possible limitations and uncertainties of RIGB method, followed by our conclusions.

2 Data

AWS used in this study are from three networks: Greenland Climate Network (GC-Net), the Kangerlussuaq transect (K-transect) and the Programme for Monitoring of the Greenland Ice Sheet (PROMICE). The first GC-Net station was set up in 1995. By 2014, there were a total of 17 long-term AWS in GC-Net, spreading in both ablation and accumulation zones (Steffen et al., 1996). Three AWS at the K-transect were initiated in 2003 (van den Broeke et al., 2011), with one more station added in 2010. Since 2007, PROMICE set up 22 AWS in succession, arranged mostly in pairs with one station in the upper ablation zone near the equilibrium line and the other at a lower elevation well into the ablation zone (van As and Fausto, 2011).

In this study, we correct the sensor tilt problem in surface SW data observed by AWS from all three aforementioned datasets during melt seasons (i.e., May–August) from 2008 to 2013, when data at most of the stations are available. Stations with more than two years of missing data are excluded from consideration, including Crawford Point1, GITS, NASA-U and Petermann Gl. from GC-Net, and MIT, QAS_A and TAS_A from PROMICE. In addition, s5, s6 and s9 from K-transect, and NUK_L from PROMICE are not included either, since the diurnal maximum of shortwave upwelling radiation (i.e., radiation reflected by surface) at these stations are at least one hour off from the solar noon. Usually, the reflected radiation is isotropic. As a result, the effect of sensor

TCD
9, 6025–6060, 2015

tilt on the shortwave upwelling radiation is mainly on the magnitude rather than the diurnal phase. An offset of this amount in the diurnal phase of shortwave upwelling radiation could be caused by highly irregular topography, specular reflection or time logger error, which cannot be corrected by RIGB. The remaining number of stations is 32, of which 13 stations are from GC-Net, one from K-transect and 18 from PROMICE (Fig. 1). The radiative flux from these datasets is hourly average. We synchronize all three datasets to account the fact that the time stamp of GC-Net and K-transect is half an hour after the interval mid-point (i.e., data stamped as 8 a.m. represent the average from 7 to 8 a.m.); the one of PROMICE is half an hour before the interval mid-point (i.e., data stamped as 8 a.m. represent the average from 8 to 9 a.m.). PROMICE also provides adjusted SW by measured tilt angles at their stations, which can be used as a reference for our method. However, this PROMICE product has not corrected the inclinometer orientation shift yet.

3 Methodology

Based on the geometric relationship between the tilted insolation observations and simulations on a horizontal surface on clear days, we deduce tilt angles and directions, and then use them to correct the tilt-induced biases on the neighboring cloudy days.

3.1 Surface radiative flux simulation

We use a Column Radiation Model (CRM), the stand-alone version of the radiation model in Community Atmosphere Model 3 (CAM3) updated from Zender (1999), to simulate surface radiative flux on clear days based on atmospheric profiles and surface conditions. Here we use atmospheric temperature profiles and humidity profiles, and surface conditions (except surface albedo) from the Atmospheric Infrared Sounder (AIRS) (AIRS Science Team/Joao Texeira, 2013). Its Infrared and Micro-Wave (IR/MW) sounding instruments retrieve reliable profiles even near the surface (Susskind et al.,

TCD
9, 6025–6060, 2015

2003). The highly heterogeneous surface albedo is the 24 h running average albedo from AWS, rather than the satellite observed surface albedo with a larger footprint. Atmospheric constituents with little variability, such as O_3, CO_2 and Aerosol Optical Depth are set to values from a sub-Arctic standard atmosphere.

3.2 Radiation on a tilted surface

SW on a tilted surface comprises of three parts: direct radiation or beam radiation ($I_{b,t}$), diffuse radiation ($I_{d,t}$) and reflected radiation from a nearby horizontal surface ($I_{r,t}$). These three parts can be calculated separately from tilt angle (β) and tilt direction (a_w), time and place, and SW on the horizontal surface (I_h), assuming isotropic reflection at the surface (Goswami et al., 2000). First, the direct radiation ($I_{b,t}$) is calculated from the direct part of SW on the horizontal surface ($I_{b,h}$) and the solar zenith angle observed on the tilted surface (i), as below:

$$I_{b,t} = I_{b,h} \times \cos i \tag{1}$$

$I_{b,h}$ is known from the true solar zenith angle (z) and the diffuse ratio (C):

$$I_{b,h} = \frac{I_h}{\cos z + C} \tag{2}$$

$\cos i$ follows the geometric relationship with the true solar zenith angle (z), solar azimuth angle (a_s), tilt angle (β) and tilt direction (a_w):

$$\cos i = \sin z \times \cos(a_s - a_w) \times \sin\beta + \cos z \times \cos\beta \tag{3}$$

We calculate solar declination used to estimate solar zenith angle (z) and azimuth angle (a_s) following algorithm from Reda and Andreas (2004). Next, the diffuse ($I_{d,t}$) and reflected radiation ($I_{r,t}$) are calculated as below:

$$I_{d,t} = C \times I_{b,h} \times (1 + \cos\beta)/2 \tag{4}$$

$$I_{r,t} = \rho \times I_h \times (1 - \cos\beta)/2 \tag{5}$$

TCD
9, 6025–6060, 2015

Where ρ is an approximation of surface albedo. A value of 0.8 is used here for snow covered ground as suggested by Goswami et al. (2000).

The relation between SW measured by the tilted sensor (I_t) and SW on the horizontal surface simulated by CRM (I_h) can be summarized as:

$$I_t = \frac{I_h}{\cos z + C} \times \left[\cos i + C \times (1 + \cos\beta)/2 + \rho \times (\cos z + C)(1 - \cos\beta)/2\right] \quad (6)$$

where C is 0.2 for insolation on clear days. The relatively larger value of C used here accounts the effects of undetected clouds (Harrison et al., 2008). For shortwave upwelling radiation, only the term of diffuse radiation is used.

3.3 Estimate of tilt angle and direction

The SW provided by the three datasets used in this study could include all the AWS measuring problems of icing, riming, shadowing, cosine response error and sensor tilt. AWS from GC-Net use the LI-COR 200SZ pyranometer, which has a better resistance to rime formation than the standard thermopile pyranometers (Stroeve et al., 2005), due to its small thermal mass. van den Broeke et al. (2004) found the Kipp and Zonen CM3 pyranometer, used by AWS from K-transect and PROMICE, is also less susceptible to riming, since it only has a single dome (rather than double domes), which can be heated up by solar radiation together with the black sensor plate to prevent rime formation. Furthermore, using only clear days with perfect cosine curves to estimate tilt angle-direction helps remove the effects of icing, riming and shadowing. To limit the effect of cosine response error, only data with a solar zenith angle less than 75° are used. We assume, therefore, the residual bias is mainly caused by sensor tilt, with an uncertainty in device measurement and random environmental noise. The best pair of tilt angle-direction, (β, a_w), is chosen as the pair which produces the surface insolation with the correct shift in phase (± 0.5 h) and the smallest absolute error in magnitude compared with CRM simulations.

TCD
9, 6025–6060, 2015

3.4 Data adjustment

The best pair of tilt angle-direction estimated using insolation on all the clear days in one month is used to adjust radiation of that whole month. Usually the variability of tilt angle-direction within a month is negligible, meaning the adjusted radiation using tilt angle-direction estimated on one clear day is as good as that using data on other clear days. However, there are cases in which tilt angle changes several degrees in one month. These situations are detected by comparing insolation adjusted using tilt angle-direction pairs estimated on different clear days, and then are processed separately if the standard deviation is larger than $5\,W\,m^{-2}$. To adjust insolation of both clear and cloudy days (i.e., calculate radiation on the horizontal surface I_h from that on the tilted surface I_t), Eq. (6) shown previously is used with the diffuse ratio (C) calculated by the cloud fraction (CF) from the Clouds and the Earth's Radiant Energy System (van As, 2011).

$$C = 0.2 + 0.8 \times CF \tag{7}$$

Since the improvements in the shortwave upwelling radiation are negligible for the tilt angle range estimated in this study, no tilt correction is performed on it. SW with a solar zenith angle larger than 75° is also adjusted with physically impossible (i.e., insolation at surface larger than at TOA; or albedo larger than 0.99) and suspicious data (i.e., a sudden change in albedo) removed. Missing data points with both adjoining sides of data available are filled with linear interpolation.

4 Validation

Station tilt affects both the phase and magnitude of the diurnal variability of surface radiative flux. The phase shift can be discerned by comparing the time of observed insolation maximum with solar noon time under clear-sky conditions. The solar noon time at one station is known from its longitude and the date. There is a frequent shift

TCD
9, 6025–6060, 2015

of maximum insolation time against solar noon in the unadjusted AWS measurements at most stations (Fig. 2). On fewer than 40 % of all clear days, insolation peaks within ±0.5 h of solar noon. Some of the shifts are larger than 3 h. On the other hand, over 60 % of the RIGB-adjusted insolation peaks at solar noon. The maximum shift is 0.5 h.

The improvements in AWS insolation are further evaluated by comparing unadjusted AWS data with RIGB-adjusted data and with the PROMICE adjustment against the Clouds and the Earth's Radiant Energy System (CERES) (CERES Science Team, 2015) and the Modern-Era Retrospective Analysis for Research and Applications (MERRA) (Rienecker et al., 2011). The AWS from PROMICE are equipped with inclinometers that record the station tilt angles. The tilt-corrected data are provided whenever inclinometers worked, with no correction on the inclinometer orientation yet. The CERES insolation is Synoptic Radiative Fluxes and Clouds (SYN) Edition-3A Level-3 data, the spatial and temporal resolution of which are 1° and 3 h, respectively. The data from MERRA are 1/2- by 2/3° hourly flux. We compare AWS observations with data in the nearest CERES and MERRA grid. Comparisons are only conducted between 6 a.m. and 6 p.m. at local solar time, since the extrapolation of data in the early mornings and late nights – when most of the data are removed due to icing/riming and low sensitivity problems – is problematic.

RIGB adjustment better agrees with both CERES and MERRA, relative to the unadjusted data and PROMICE adjustment (Fig. 3). At PROMICE stations, the RIGB Root-Mean-Square-Errors (RMSE) against CERES and MERRA are ~ 20 $W m^{-2}$ smaller than the RMSE of the unadjusted data, and are also smaller than the RMSE of the PROMICE adjustment (Fig. 3a and b). Correlations of RIGB with CERES and MERRA are the strongest. Their correlation coefficients exceed 0.97 for both references, in contrast with the low values of the unadjusted data, which are 0.92 for CERES and 0.94 for MERRA. The ones of PROMICE adjustment are in-between: 0.95 for CERES and 0.96 for MERRA. The RIGB-adjusted insolation also better agrees with the references at GC-net and K-transect stations, with ~ 10 $W m^{-2}$ less RMSE relative to the unadjusted data, and correlation coefficients over 0.96 (Fig. 3c and d). Under

TCD
9, 6025–6060, 2015

all-sky conditions, the improvements in RMSE are over 20 $W m^{-2}$ for both CERES and MERRA, although the absolute biases are larger (Table 1).This large bias could be caused by the inaccurate estimates of cloud properties by the satellite instrument (i.e., CERES) and reanalysis (i.e., MERRA). We noticed a systematic difference in insolation between CERES and MERRA, which is $\sim 10\,W m^{-2}$ under clear-sky conditions and $\sim 30\,W m^{-2}$ on cloudy days. RIGB adjustment is consistently accurate when compared to either CERES or MERRA, because our adjustment is on the daily time-scale, which is shorter than that of the systematic difference.

To illustrate the agreement between the PROMICE measured and RIGB estimated tilt angles, we next compare these angles at Station KPC_U, where the station rotation is small according to the field notes taken on revisits. The hourly north-south and east-west tilt angles measured by inclinometers are converted to tilt angle-direction format, assuming no station rotation, and then averaged over a month. The measured and estimated tilt angle-direction agree reasonably well (Fig. 4). The year-to-year relative positions are the same. The maximum absolute differences in the tilt angle and direction are 1.95° and 33.67°, with the averages of 0.72° and 11.23°, respectively.

The largest improvement of our tilt correction (i.e., RIGB adjustment minus unadjusted data) occurs at South Dome, with a daily average of 51 $W m^{-2}$ under all-sky conditions and 79 $W m^{-2}$ under clear-sky conditions. Although the tilt angles are more variable in the ablation zone (i.e., altitude < 2000 m), the absolute values are larger in the accumulation zone (i.e., altitude > 2000 m), caused by the large systematic tilt at each of the southern stations. Therefore, our method improves the insolation more in the accumulation zone (19 $W m^{-2}$) than in the ablation zone (16 $W m^{-2}$; Table 2). The average daily improvement of all stations under all-sky conditions is $18 \pm 13\,W m^{-2}$, which is equivalent to a snow melt in liquid of 0.40 ± 0.29 m throughout the melt season, using an albedo of 0.7.

TCD
9, 6025–6060, 2015

5 Impact on snow surface albedo

Snow albedo controls the absorbed solar radiation at the surface. Short-term changes in albedo can lead to snow-melt and trigger the positive snow-albedo feedbacks. Little is known about the sub-daily variabilities of albedo in the Arctic, due to a lack of high-temporal-resolution satellite observations and reliable in situ measurements. Although the polar-orbiting satellites such as MODIS pass through parts of Greenland several times a day, only daily average albedo is available because of cloud interference. The cosine response error and the sensor tilt can introduce false diurnal fluctuations into AWS observed albedo. In climate models, the diurnal change of snow albedo is typically estimated by solar zenith angle and snow grain size (van den Broeke et al., 2004). In reality, more factors contribute to this diurnal change, including internal properties (such as particle shape and snow density) and external factors (such as solar azimuth angle and topography) (Flanner and Zender, 2006; Wang and Zender, 2011). With the tilt-corrected radiation, we find a more consistent diurnal change in surface albedo. For example, the semi-smiling curves of albedo are smoother using the adjusted data (Fig. 5a and b). At stations with large tilt angles, RIGB adjusts the diurnal variability patterns from frowning to smiling (Fig. 5c and d).

Sometimes, the pyranometer tilts enough to jeopardize the daily average albedo, which in turn impacts climatology on long-term time scales. For example, at Station UPE_L in Northwest Greenland, the tilt angle jumped from 2° to 9° from June to July of 2010. Without tilt correction, data show an improbably higher albedo in July than in June (Fig. 6a), which contradicts the results from a nearby station, UPE_U (Fig. 6b), as well as the concurrent temperature trend. The high monthly average albedo in the unadjusted data in July 2010 was caused by the abnormally high values in the early mornings and late evenings, due to a shift in downwelling radiation against the upwelling. This misleading effect cannot be fully removed by either the 24 h running average or limiting the solar zenith angle to less than 75°. After the tilt effect is countered, the normal climatology is restored.

TCD
9, 6025–6060, 2015

Sensor tilt can also affect the inter-annual variability of albedo. In 2012, Greenland experienced the largest melt extent in the satellite era since 1979 (Nghiem et al., 2012), which is seen as an epic low albedo in both unadjusted and RIGB-adjusted data in the accumulation zone (Fig. 7a). In this area, melt only occurs during a limited period of time in the summer, and thus the tilt problem is not as serious as in the ablation zone. In the ablation zone, the unadjusted data shows the smallest albedo in 2010 instead of in 2012. Moreover, the between-station variability of the unadjusted data is almost 5 times larger than that of the RIGB-adjusted data (shown by the error bars in Fig. 7b), indicating varied tilt effects at different stations. After the tilt correction, the long-term trend and the albedo minimum are in agreement with the estimates from the NASA MOD10A data (Box, 2015).

6 Discussion

6.1 Station tilt

Of all the stations examined here, only KAN_B from PROMICE is anchored into rock; all others are anchored into glacier ice. The estimated tilt angle-directions reveal large temporal and spatial varieties. At the GC-Net stations, there is a systematic tilt direction at each station in the accumulation zone. For example, the station at South Dome always tilts to the North, and the one at DYE-2 to the Northwest. With regards to the tilt angle, both the station maximum and the temporal variability are larger in the ablation zone than in the accumulation zone, except for Station South Dome. At the PROMICE stations, there is no obvious systematic tilt direction. The tilt angles and their temporal variabilities are generally larger at the southern stations than in the northern stations. It seems that the tilt angles are less variable at GC-Net stations which use long poles as station masts than at PROMICE stations which use tripods instead. However, most GC-Net stations are in the colder accumulation zone, whereas all the PROMICE stations are in the warmer ablation zone. We also compare the temporal variability of tilt angles

TCD
9, 6025–6060, 2015

between the paired stations from PROMICE. The station at a higher altitude always has a smaller tilt angle standard deviation than the station at a lower altitude. In addition, the largest and most variable tilt angles are found in July when the snow melt intensity is strongest of the melt season (i.e., May–August). These all suggest a causal correlation between surface melt/compaction and station tilt.

Since snow melt intensity is not available at all AWS, surface albedo instead is used to compare with the tilt angle variability (Fig. 9). The significant correlation between surface albedo and station tilt variability is negative. The stations that are more northernly, at higher altitudes and with higher albedo are less affected by station tilt, whereas stations more southernly, at lower altitudes and with lower albedo are more affected. However, whether stations will tilt, and to what degree and direction also depend on environmental factors. For example, if the areas around all the anchors melt at a similar rate, the station tilt may not be as serious as one with melting that occurs only in the area around one anchor. This may explain why the correlation coefficient is relatively low (−0.60). The significant correlation between near-surface atmospheric temperature and the station tilt variability is negative as well (−0.51). The fact that thermometers from different projects are not set to the same height above the surface may contribute to this lower coefficient. Nevertheless, it is highly probable that the station tilt is controlled by surface melt/compaction. As the tilt angle gets larger, more environmental factors take effect.

We also found a weak negative correlation between station tilt and wind speed (i.e., the higher the wind speed, the smaller the tilt variability). However, this could be explained by the co-occurrence of high albedo and high wind speed at high-altitude stations. Moreover, no correlation is found between the systematic tilt directions of GC-Net stations in the accumulation zone and their dominating wind directions. These systematic tilt directions could be a result of the local slopes or station leveling problems introduced at set-up.

TCD
9, 6025–6060, 2015

6.2 Dependence on clear days

RIGB method requires clear days to perform the tilt estimation. With current precision, at least one clear day is needed per month. Among all the 768 station-months used in this study (i.e., 32 stations, 6 years per station and 4 months per year), there are 25 station-months (3.26 %) with no clear days to use. However, most of these (24 out of 25) have at least half of the AWS measurements missing. Only 1 of the 768 station-months was too cloudy to have any clear days. We provide no correction during those months. Another potential limit of RIGB is that it requires more clear days to accurately capture station tilt when the inter-month variability is large.

6.3 Uncertainty in the tilt-corrected insolation

The surface insolation simulation using CRM driven by AIRS profiles under clear-sky conditions are validated against Atmospheric Radiation Measurements (ARM) at Barrow, Alaska, USA (Atmospheric Radiation Measurement (ARM) Climate Research Facility, 1994). Since we use a constant Aerosol Optical Depth (AOD), only insolation in May is used in order to eliminate the interference of wild fires. From 2008 to 2013, the hourly average difference between the measured and simulated insolation is $5 \pm 3\,\mathrm{W\,m^{-2}}$, which is less than 2 ± 1 % of the daily average.

The data quality of the tilt-corrected insolation under all-sky conditions also relies on the quality of cloud fraction data. Higher cloud fraction results in a higher diffuse ratio (C). With more isotropic diffuse radiation, insolation is less susceptible to station tilt. Therefore, if the cloud fraction is under-estimated, the insolation will be over-corrected; vice versa. In the Arctic, the fast-changing convective clouds are rare, so we use the 3 hourly cloud fraction from CERES. With regards to the cloud radiative properties, CERES estimates are reasonably accurate (Minnis et al., 2011). In the Arctic, the average difference between the in situ ground-measured and CERES cloud fraction is ~ 0.15 (Minnis et al., 2008). The effect of cloud fraction on the insolation adjustment depends on both the tilt angle and tilt direction (Fig. 10). The adjustment at local solar

TCD
9, 6025–6060, 2015

noon is largest when the station tilts to the North ($a_w = 180^\circ$) or South ($a_w = 0^\circ$). The maximum of daily average turns clockwise, e.g., to $a_w = 30^\circ$ and $a_w = -150^\circ$ when the tilt angle (β) is 10°. The cloud fraction uncertainty of 0.15 can cause an uncertainty in insolation adjustment up to 7.5 W m^{-2} when cloud fraction is close to 0. The effect becomes smaller, when cloud fraction is close to 1. The tilt correction is larger as the station tilts more (Fig. 10b). In 90 % of the station-months we used, the tilt angles are less than 10°, 95 % less than 15°. Therefore, the uncertainty in insolation adjustment caused by the uncertainty in cloud fraction should be well under 10 W m^{-2}, considering an average cloud fraction of 0.81 in the Arctic during summertime (Vavrus et al., 2008). Nevertheless, a cloud fraction dataset with a higher resolution would further benefit the quality of the hourly radiation measurements from AWS.

7 Conclusions

In this study, we identify and correct the SW tilt bias using tilt angles and directions estimated by comparing CRM simulated insolation with AWS observed insolation under clear-sky conditions. Station tilt causes considerable bias in insolation. On fewer than 40 % of clear days, the unadjusted insolation peaks at the correct solar noon time (±0.5 h). The largest bias exceeds 3 h. The unadjusted insolation RMSE against CERES and MERRA at all stations are as large as ∼ 70 W m^{-2} under clear-sky conditions, with a correlation coefficient of ∼ 0.90. Using the estimated tilt angle-directions, which are in a good agreement with the measured tilt angles, RIGB adjustment reduces the RMSE by ∼ 20 W m^{-2}, and enhances the correlation coefficients to above 0.96. The overall improvement relative to the unadjusted data under all-sky conditions is 18 ± 13 W m^{-2}, which is enough to melt 0.40 ± 0.29 m snow water equivalent using an albedo of 0.7. With this tilt-corrected SW data, we found a consistent semi-smiling diurnal cycle of albedo in Greenland. The derived seasonal and inter-annual variabilities of albedo agree better with satellite observations and temperature changes. This RIGB tilt correction method relies only on the iterative

TCD
9, 6025–6060, 2015

application of solar geometric principles, that requires no additional instrumentation. Therefore, it can retrospectively solve the tilt problems in SW measurement, and provides multi-year consistent SW for the analysis of surface energy budgets and melt as well as validation of satellite observations and model simulations on Greenland Ice Sheet and in other snow-covering areas.

Acknowledgements. W. Wang thanks Carolyn McClaskey for her constructive feedbacks. The authors acknowledge the GC-Net team for providing and helping to interpret AWS measurements. CERES cloud and radiation data were obtained from the NASA Langley Research Center Atmospheric Science Data Center; MERRA radiation data were obtained from the Global Modeling and Assimilation Office and the Goddard Earth Sciences Data and Information Services Center. This work was funded by NASA Grants NNX12AF48A and NNX14AH55A.

References

AIRS Science Team/Joao Texeira: Aqua AIRS Level 2 Support Retrieval (AIRS+AMSU), version 006, NASA Goddard Earth Science Data and Information Services Center (GES DISC), Greenbelt, MD, USA, doi:10.5067/AQUA/AIRS/DATA207, 2013. 6032

Andersen, M., Stenseng, L., Skourup, H., Colgan, W., Khan, S., Kristensen, S., Andersen, S., Box, J., Ahlstrøm, A., Fettweis, X., and Forsberg, R.: Basin-scale partitioning of Greenland ice sheet mass balance components (2007–2011), Earth Planet. Sc. Lett., 409, 89–95, doi:10.1016/j.epsl.2014.10.015, 2015. 6028

Atmospheric Radiation Measurement (ARM) Climate Research Facility: Data Quality Assessment for ARM Radiation Data (QCRAD1LONG), 2008-05-01 to 2013-05-31, 71.323 N 156.609 W: North Slope Alaska (NSA) Central Facility, Barrow AK (C1), Oak Ridge, Tennessee, USA, compiled by: Shi, Y. and Riihimaki, L., doi:10.5439/1027372, 1994.

Bogren, W. S., Burkhart, J. F., and Kylling, A.: Tilt error in cryospheric surface radiation measurements at high latitudes: a model study, The Cryosphere Discuss., 9, 4355–4376, doi:10.5194/tcd-9-4355-2015, 2015. 6030

TCD
9, 6025–6060, 2015

Box, J. E.: Greenland melt season kicks off slowly in 2015; the new abnormal, available at: http://www.meltfactor.org/blog/greenland-melt-season-kicks-off-slowly-in-2015/, last access: 1 July 2015. 6039

Box, J. E., Fettweis, X., Stroeve, J. C., Tedesco, M., Hall, D. K., and Steffen, K.: Greenland ice sheet albedo feedback: thermodynamics and atmospheric drivers, The Cryosphere, 6, 821–839, doi:10.5194/tc-6-821-2012, 2012. 6029

CERES Science Team: CERES SYN1deg-3Hour, Ed3A, NASA Atmospheric Science Data Center (ASDC), Hampton, VA, USA, doi:10.5067/Terra+Aqua/CERES/SYN1deg3HOUR_L3.003A, 2015. 6036

Enderlin, E. M., Howat, I. M., Jeong, S., Noh, M.-J., van Angelen, J. H., and van den Broeke, M. R.: An improved mass budget for the Greenland ice sheet, Geophys. Res. Lett., 41, 866–872, doi:10.1002/2013GL059010, 2014. 6028

Fettweis, X.: Reconstruction of the 1979–2006 Greenland ice sheet surface mass balance using the regional climate model MAR, The Cryosphere, 1, 21–40, doi:10.5194/tc-1-21-2007, 2007. 6029

Flanner, M. G. and Zender, C. S.: Linking snowpack microphysics and albedo evolution, J. Geophys. Res., 111, D12208, doi:10.1029/2005JD006834, 2006. 6038

Goswami, D., Kreith, F., and Kreider, J.: Radiation on tilted surface, in: Principles of Solar Engineering, 2nd Edn., Taylor and Francis, Philadelphia, PA, USA, 47–48, 2000. 6033, 6034

Harrison, R. G., Chalmers, N., and Hogan, R. J.: Retrospective cloud determinations from surface solar radiation measurements, Atmos. Res., 90, 54–62, doi:10.1016/j.atmosres.2008.04.001, 2008. 6034

Kuipers Munneke, P., Reijmer, C. H., and van den Broeke, M. R.: Assessing the retrieval of cloud properties from radiation measurements over snow and ice, Int. J. Climatol., 31, 756–769, doi:10.1002/joc.2114, 2011. 6029

Minnis, P., Trepte, Q. Z., Sun-Mack, S., Chen, Y., Doelling, D. R., Young, D. F., Spangenberg, D. A., Miller, W. F., Wielicki, B. A., Brown, R. R., Gibson, S. C., and Geier, E. B.: Cloud detection in nonpolar regions for CERES using TRMM VIRS and Terra and Aqua MODIS data, IEEE T. Geosci. Remote, 46, 3857–3884, doi:10.1109/TGRS.2008.2001351, 2008. 6041

Minnis, P., Sun-Mack, S., Chen, Y., Khaiyer, M. M., Yi, Y., Ayers, J. K., Brown, R. R., Dong, X., Gibson, S. C., Heck, P. W., Lin, B., Nordeen, M. L., Nguyen, L., Palikonda, R., Smith, W. L., Spangenberg, D. A., Trepte, Q. Z., and Xi, B.: CERES edition-2 cloud

TCD
9, 6025–6060, 2015

property retrievals using TRMM VIRS and Terra and Aqua MODIS data-Part II: Examples of average results and comparisons with other data, IEEE T. Geosci. Remote, 49, 4401–4430, doi:10.1109/TGRS.2011.2144602, 2011. 6041

Nghiem, S. V., Hall, D. K., Mote, T. L., Tedesco, M., Albert, M. R., Keegan, K., Shuman, C. A., DiGirolamo, N. E., and Neumann, G.: The extreme melt across the Greenland ice sheet in 2012, Geophys. Res. Lett., 39, L20502, doi:10.1029/2012GL053611, 2012. 6028, 6039

Pithan, F. and Mauritsen, T.: Arctic amplification dominated by temperature feedbacks in contemporary climate models, Nat. Geosci., 7, 181–184, doi:10.1038/ngeo2071, 2014. 6028

Reda, I. and Andreas, A.: Solar position algorithm for solar radiation applications, Sol. Energy, 76, 577–589, doi:10.1016/j.solener.2003.12.003, 2004. 6033

Rienecker, M. M., Suarez, M. J., Gelaro, R., Todling, R., Bacmeister, J., Liu, E., Bosilovich, M. G., Schubert, S. D., Takacs, L., Kim, G.-K., Bloom, S., Chen, J., Collins, D., Conaty, A., da Silva, A., Gu, W., Joiner, J., Koster, R. D., Lucchesi, R., Molod, A., Owens, T., Pawson, S., Pegion, P., Redder, C. R., Reichle, R., Robertson, F. R., Ruddick, A. G., Sienkiewicz, M., and Woollen, J.: MERRA: NASA's modern-era retrospective analysis for research and applications, J. Climate, 24, 3624–3648, doi:10.1175/JCLI-D-11-00015.1, 2011. 6036

Schaaf, C. B., Wang, Z., and Strahler, A. H.: Commentary on Wang and Zender MODIS snow albedo bias at high solar zenith angles relative to theory and to in situ observations in Greenland, Remote Sens. Environ., 115, 1296–1300, doi:10.1016/j.rse.2011.01.002, 2011. 6028

Steffen, C., Box, J., and Abdalati, W.: Greenland Climate Network: GC-Net, edited by: Colbeck, S. C., CRREL Special Report, US Army Cold Regions Reattach and Engineering (CRREL), NTIS, Springfield, Virginia, 98–103, 1996. 6031

Stroeve, J. C., Box, J. E., Fowler, C., Haran, T., and Key, J.: Intercomparison between in situ and AVHRR polar pathfinder-derived surface albedo over Greenland, Remote Sens. Environ., 75, 360–374, doi:10.1016/S0034-4257(00)00179-6, 2001. 6029

Stroeve, J., Box, J. E., Gao, F., Liang, S., Nolin, A., and Schaaf, C.: Accuracy assessment of the MODIS 16-day albedo product for snow: comparisons with Greenland in situ measurements, Remote Sens. Environ., 94, 46–60, doi:10.1016/j.rse.2004.09.001, 2005. 6029, 6034

Stroeve, J., Box, J. E., Wang, Z., Schaaf, C., and Barrett, A.: Re-evaluation of MODIS MCD43 Greenland albedo accuracy and trends, Remote Sens. Environ., 138, 199–214, doi:10.1016/j.rse.2013.07.023, 2013. 6028, 6029, 6030

TCD
9, 6025–6060, 2015

Susskind, J., Barnet, C., and Blaisdell, J.: Retrieval of atmospheric and surface parameters from AIRS/AMSU/HSB data in the presence of clouds, IEEE T. Geosci. Remote, 41, 390–409, doi:10.1109/TGRS.2002.808236, 2003. 6032

Tedesco, M., Fettweis, X., Mote, T., Wahr, J., Alexander, P., Box, J. E., and Wouters, B.: Evidence and analysis of 2012 Greenland records from spaceborne observations, a regional climate model and reanalysis data, The Cryosphere, 7, 615–630, doi:10.5194/tc-7-615-2013, 2013. 6028

van As, D.: Warming, glacier melt and surface energy budget from weather station observations in the Melville Bay region of northwest Greenland, J. Glaciol., 57, 208–220, doi:10.3189/002214311796405898, 2011. 6029, 6030, 6035

van As, D. and Fausto, R. S.: Programme for monitoring of the Greenland Ice Sheet (PROMICE): first temperature and ablation records, Geol. Surv. Den. Greenl., 23, 73–76, 2011. 6031

van As, D., Andersen, M. L., Petersen, D., Fettweis, X., Van Angelen, J. H., Lenaerts, J. T., Van Den Broeke, M. R., Lea, J. M., Bøggild, C. E., Ahlstrøm, A. P., and Steffen, K.: Increasing meltwater discharge from the Nuuk region of the Greenland ice sheet and implications for mass balance (1960–2012), J. Glaciol., 60, 314–322, doi:10.3189/2014JoG13J065, 2014. 6029

van den Broeke, M., van As, D., Reijmer, C., and van de Wal, R.: Assessing and improving the quality of unattended radiation observations in Antarctica, J. Atmos. Ocean. Tech., 21, 1417–1431, doi:10.1175/1520-0426(2004)021<1417:AAITQO>2.0.CO;2, 2004. 6029, 6030, 6034, 6038

van den Broeke, M., Bamber, J., Ettema, J., Rignot, E., Schrama, E., van de Berg, W. J., van Meijgaard, E., Velicogna, I., and Wouters, B.: Partitioning recent Greenland mass loss, Science, 326, 984–986, doi:10.1126/science.1178176, 2009. 6028

van den Broeke, M. R., Smeets, C. J. P. P., and van de Wal, R. S. W.: The seasonal cycle and interannual variability of surface energy balance and melt in the ablation zone of the west Greenland ice sheet, The Cryosphere, 5, 377–390, doi:10.5194/tc-5-377-2011, 2011. 6028, 6031

Vavrus, S., Waliser, D., Schweiger, A., and Francis, J.: Simulations of 20th and 21st century Arctic cloud amount in the global climate models assessed in the IPCC AR4, Clim. Dynam., 33, 1099–1115, doi:10.1007/s00382-008-0475-6, 2008. 6028, 6042

TCD
9, 6025–6060, 2015

Velicogna, I. and Wahr, J.: Time-variable gravity observations of ice sheet mass balance: precision and limitations of the GRACE satellite data, Geophys. Res. Lett., 40, 3055–3063, doi:10.1002/grl.50527, 2013. 6028

Wang, X. and Zender, C. S.: Constraining MODIS snow albedo at large solar zenith angles: implications for the surface energy budget in Greenland, J. Geophys. Res., 115, F04015, doi:10.1029/2009JF001436, 2010a. 6028

Wang, X. and Zender, C. S.: MODIS snow albedo bias at high solar zenith angles relative to theory and to in situ observations in Greenland, Remote Sens. Environ., 114, 563–575, doi:10.1016/j.rse.2009.10.014, 2010b. 6028

Wang, X. and Zender, C. S.: Arctic and Antarctic diurnal and seasonal variations of snow albedo from multiyear Baseline Surface Radiation Network measurements, J. Geophys. Res., 116, F03008, doi:10.1029/2010JF001864, 2011. 6038

Zender, C. S.: Global climatology of abundance and solar absorption of oxygen collision complexes, J. Geophys. Res., 104, 24471, doi:10.1029/1999JD900797, 1999. 6032

TCD
9, 6025–6060, 2015

Table 1. RMSE of AWS against the reference datasets under all-sky conditions (W m^{-2}).

AWS	Reference	Unadjusted	PROMICE Adjustment	RIGB Adjustment
PROMICE	CERES	146	115 (−21 %)	100 (−32 %)
	MERRA	175	153 (−13 %)	149 (−15 %)
GC-Net and K-transect	CERES	93		72 (−23 %)
	MERRA	102		90 (−12 %)

Numbers in the parentheses are the percentage of changes relative to the unadjusted data.

TCD
9, 6025–6060, 2015

Table 2. Daily average improvements in insolation.

Zone	Condition	Unadjusted ($W\ m^{-2}$)	RIGB adjustment ($W\ m^{-2}$)	Absolute difference* ($W\ m^{-2}$)	
Accumulation	All-Sky	297	362	19	(6 %)
	Clear-Sky	326	402	52	(16 %)
Ablation	All-Sky	283	320	16	(6 %)
	Clear-Sky	343	424	43	(12 %)

Numbers in the parentheses are the percentages of the absolute differences relative to the unadjusted insolation.
* Hourly Average of absolute difference between unadjusted data and RIGB adjustment, not the difference between Column 3 and 4.

TCD
9, 6025–6060, 2015

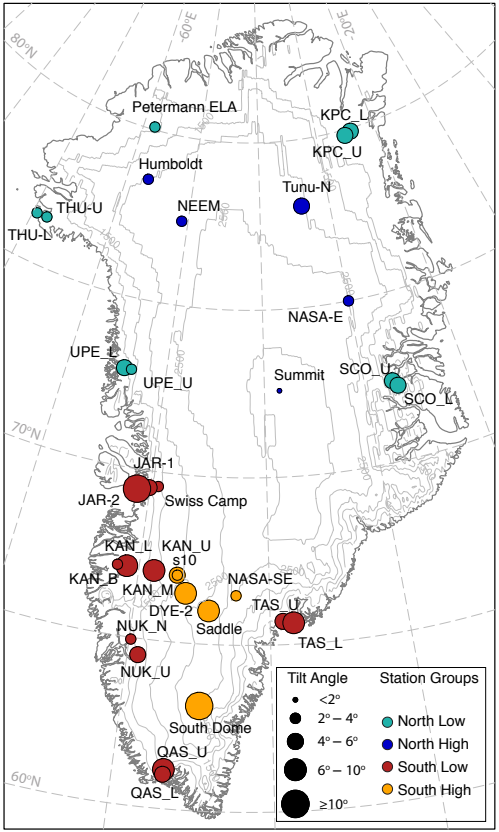

Figure 1. The Automatic Weather Stations used in this study and their average tilt angles (β). Stations are separated into four groups based on their latitudes and altitudes.

TCD
9, 6025–6060, 2015

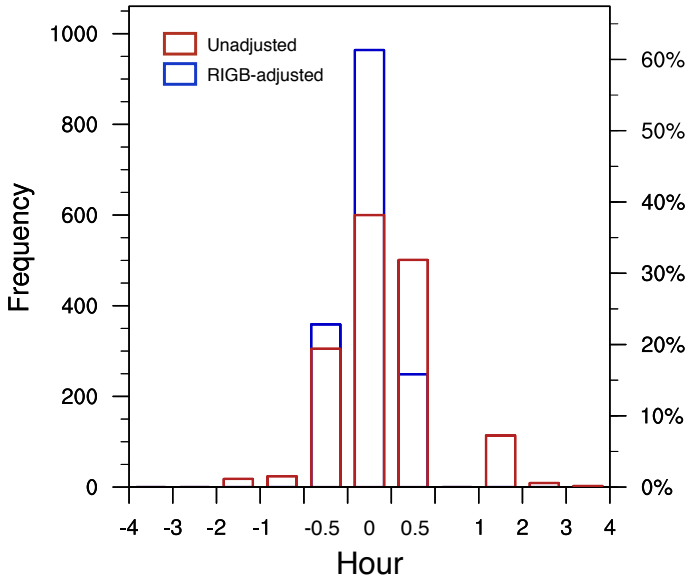

Figure 2. Shifts of maximum insolation time to solar noon in unadjusted data and RIGB adjustment. The precision of the solar noon time is 0.5 h.

TCD
9, 6025–6060, 2015

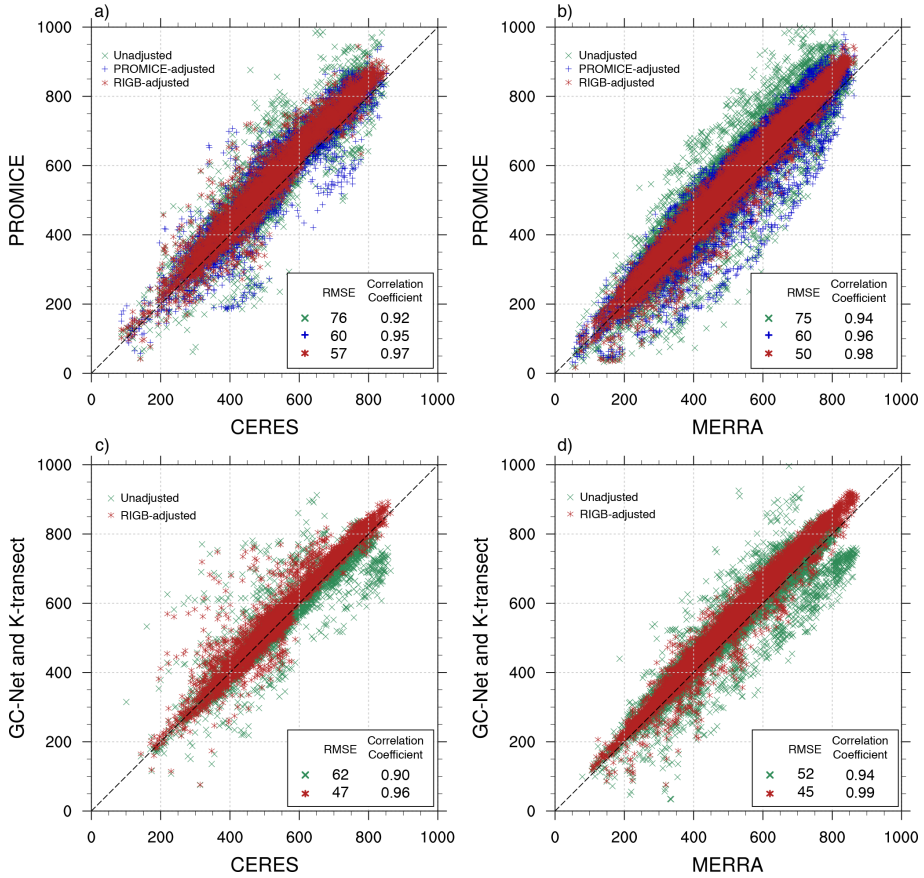

Figure 3. Correlation of insolation (W m^{-2}) between **(a)** PROMICE with CERES; **(b)** PROMICE with MERRA; **(c)** GC-Net and K-transect with CERES; **(d)** GC-Net and K-transect with MERRA.

TCD
9, 6025–6060, 2015

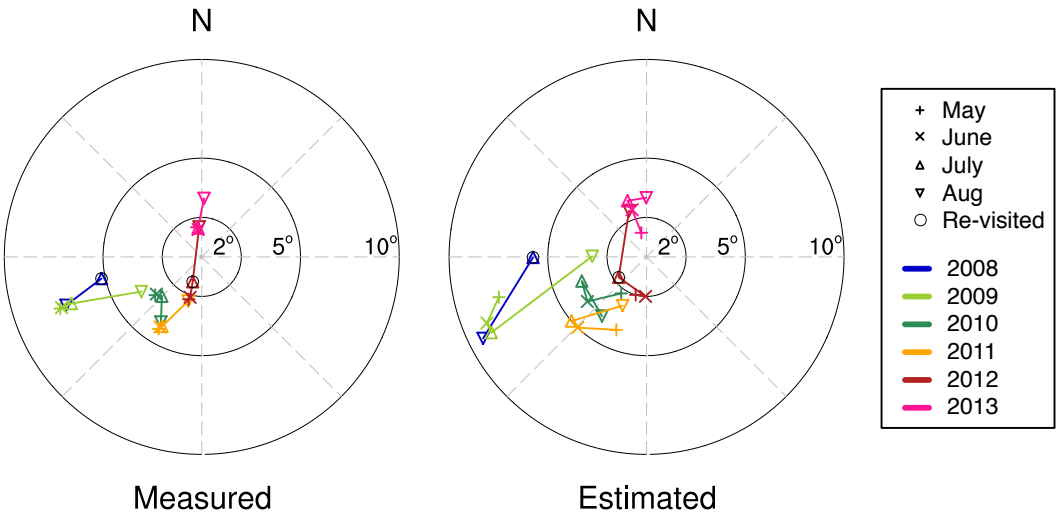

Figure 4. Measured and estimated tilt angle-direction at Station KPC_U. The distance from the circle center represents the station tilt angle (β). The direction represents the station tilt direction (a_w) with 0° pointing to the South. The markers are circled in black if the station was re-visited in those months.

TCD
9, 6025–6060, 2015

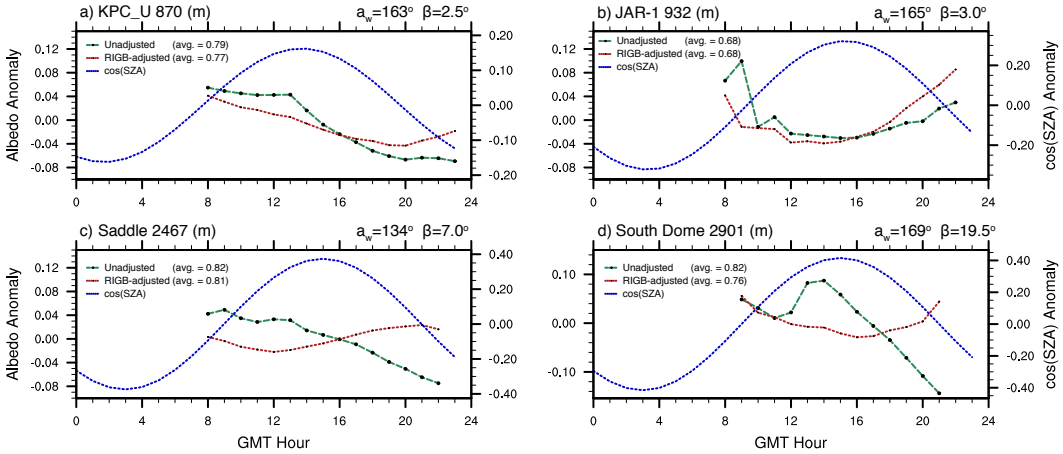

Figure 5. Diurnal variability of albedo at SZA less than 75° in June 2013 at **(a)** KPC_U; **(b)** JAR-1; **(c)** Saddle; **(d)** South Dome. The station altitude and tilt angle-direction are labeled on the top of each panel.

TCD
9, 6025–6060, 2015

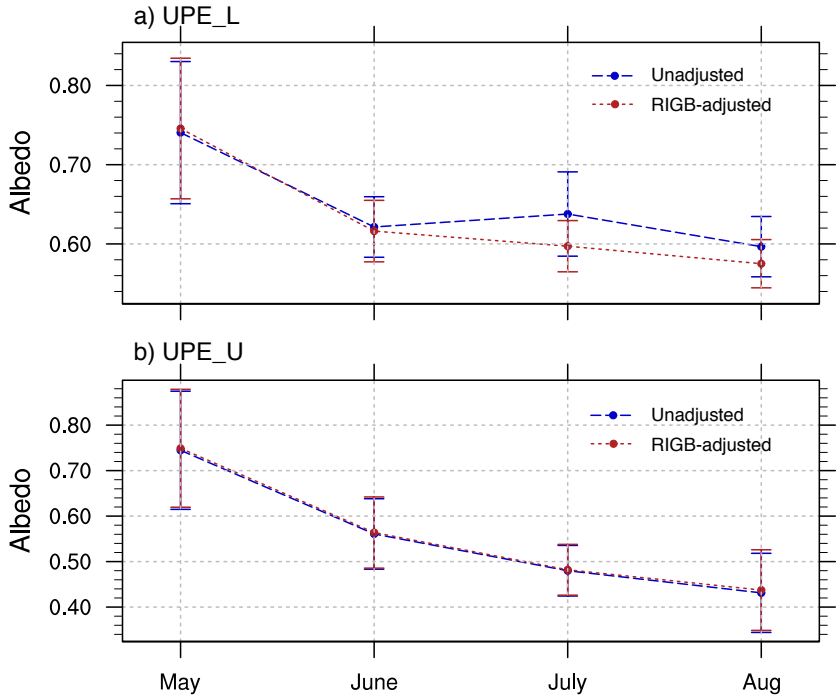

Figure 6. Monthly average albedo at **(a)** UPE_L and **(b)** UPE_U in May–August 2010 with standard deviation as error bars.

TCD
9, 6025–6060, 2015

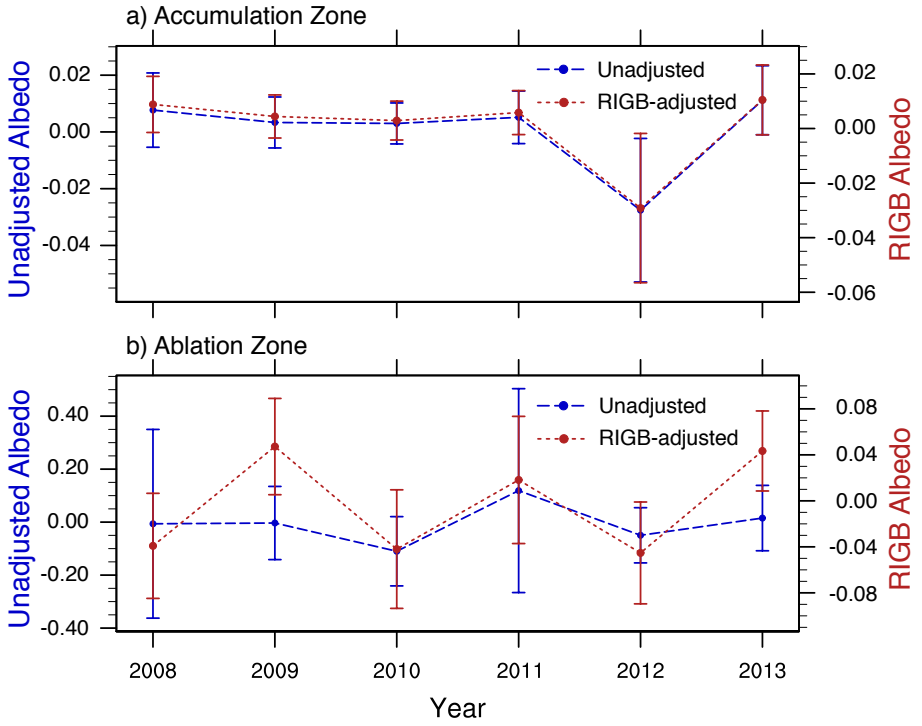

Figure 7. Annual average albedo using unadjusted data (on the left *Y* axis) and RIGB-adjusted data (on the right *Y* axis) in **(a)** accumulation zone; **(b)** ablation zone with standard deviation as error bars.

TCD
9, 6025–6060, 2015

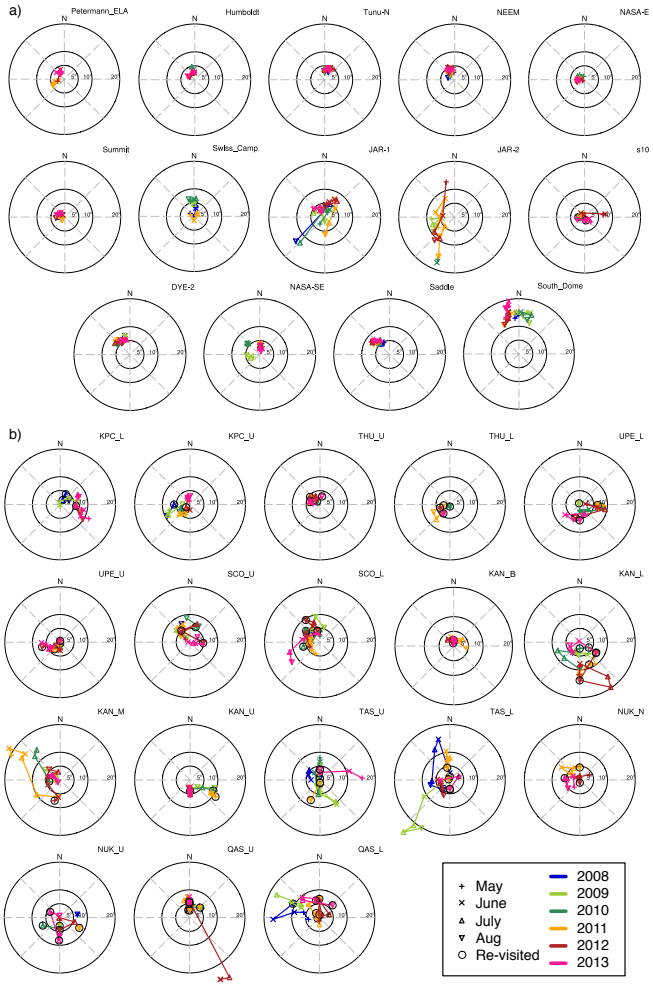

TCD
9, 6025–6060, 2015

RIGB tilt correction method for radiation, Greenland

W. Wang et al.

Figure 8. Station tilt angles (represented by the distance from the circle center) and tilt directions (0° points to the South) of **(a)** GC-Net and K-transect; **(b)** PROMICE. The markers are circled in black if the stations were re-visited in those months (no re-visiting record for GC-Net is found). There might be multiple tilt angles in one month. The panels of stations on each sub-figure are arranged in the order of latitude, from North to South.

TCD
9, 6025–6060, 2015

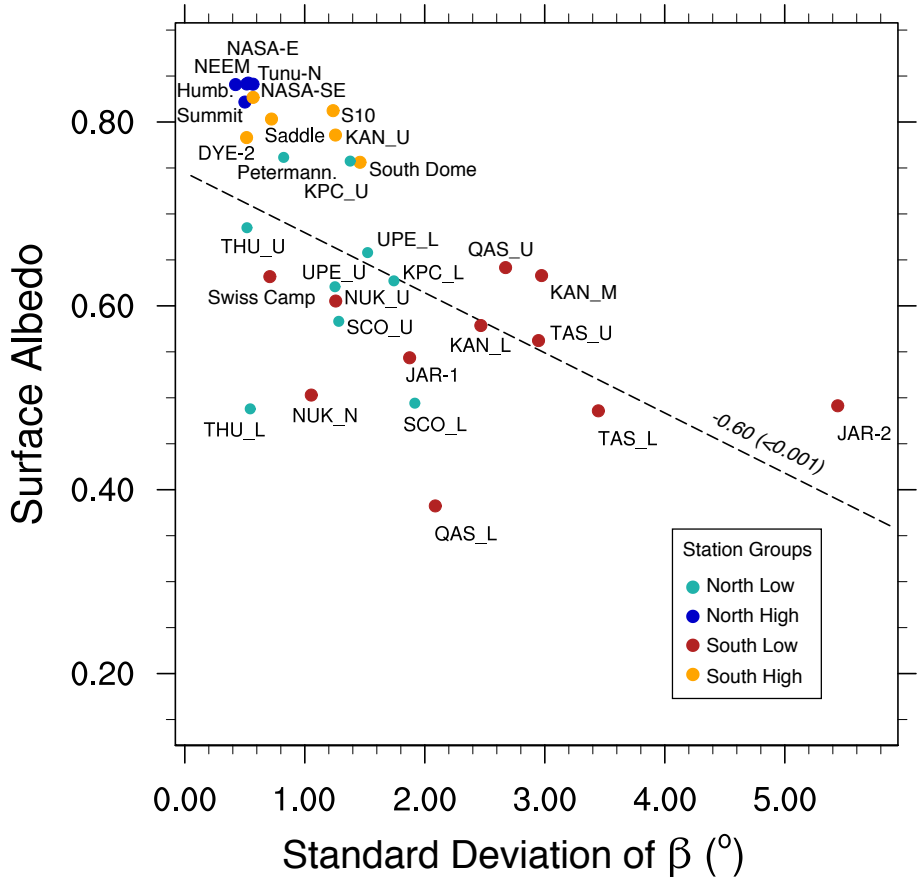

Figure 9. Correlation between surface albedo and the standard deviation of tilt angles (β). Numbers on dashed lines are the correlation coefficient with the significant level in parentheses (using a two-tailed t test). Station KAN_B that is anchored into rock is not included.

TCD
9, 6025–6060, 2015

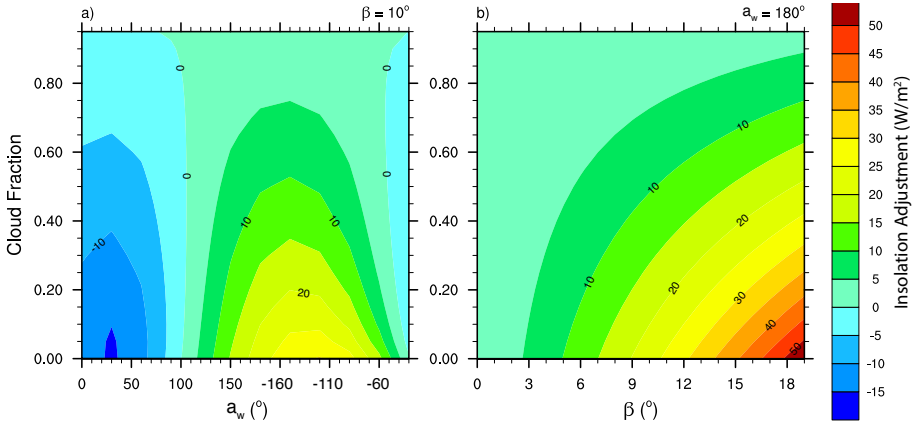

Figure 10. The effect of cloud fraction on daily average tilt correction of insolation changing with **(a)** tilt direction (a_w) and **(b)** tilt angle (β).

TCD
9, 6025–6060, 2015